DISTRIBUTION STATEMENT A. Approved for public release; distribution is unlimited.

Extended-Range Prediction with Low-Dimensional, Stochastic-Dynamic Models: A Data-driven Approach

Michael Ghil (PI), Mickaël D. Chekroun and Dmitri Kondrashov
Dept. of Atmospheric & Oceanic Sciences and Institute of Geophysics and Planetary Physics,
University of California, Los Angeles, CA
603 Charles E. Young Dr., East, 3845 Slichter Hall, Los Angeles, CA 90095-1567
Ghil phone: (310) 825-1038 fax: (310) 206-5219 email:ghil@atmos.ucla.edu
Chekroun phone: (310) 825-1038 fax: (310) 206-5219 email:mchekroun@atmos.ucla.edu
Kondrashov phone: (310) 825-1038 fax: (310) 206-5219 email:dkondras@atmos.ucla.edu

Michael K. Tippett (CU coordinator), Andrew W. Robertson, Suzana J. Camargo, Mark Cane, Dake Chen, Alexey Kaplan, Yochanan Kushnir, Adam Sobel, Mingfang Ting, Xiaojun Yuan
Columbia University, Lamont Campus 61 Route 9W, Palisades New York 10964, USA.
Tippett phone: (845) 680-4420 fax: (845) 680-4866 email:tippett@columbia.edu
Robertson phone: (845) 680-4491 fax: (845) 680-4866 email:awr@columbia.edu
Camargo phone: (845) 365-8640 fax: (845) 365-8157 email:suzana@ldeo.columbia.edu
Cane phone: (845) 365-8344 fax: (845) 365-8157 email:mcane@ldeo.columbia.edu
Chen phone: (845) 365-8496 fax: (845) 365-8157 email:dchen@ldeo.columbia.edu
Kaplan phone: (845) 365-8689 fax: (845) 365-8157 email:alexeyk@ldeo.columbia.edu
Kushnir phone: (845) 365-8669 fax: (845) 365-8157 email:kushnir@ldeo.columbia.edu
Sobel phone: (845) 365-8527 fax: (845) 365-8157 email:ahs129@columbia.edu
Ting phone: (845) 365-8374 fax: (845) 365-8157 email:ting@ldeo.columbia.edu
Yuan phone: (845) 365-8820 fax: (845) 365-8157 email:xyuan@ldeo.columbia.edu

Award Number: N00014-12-1-0911
http://www.onr.navy.mil/sci_tech/32/reports/annual/

LONG-TERM GOALS

The long-term goal of this project is to quantify the extent to which reduced-order models can be used for the description, understanding and prediction of atmospheric, oceanic and sea ice variability on time scales of 1–12 months and beyond.

OBJECTIVES

Demonstrate the ability of linear and nonlinear, stochastic-dynamic models to capture the dominant and most predictable portion of the climate system's variability. Improve the understanding and prediction of the low-frequency modes (LFMs) of variability such as the Madden-Julian Oscillation (MJO), El Niño–Southern Oscillation (ENSO), North Atlantic Oscillation (NAO) and Pacific–North American (PNA) pattern. Validate LDMs based on data sets from observations, reanalyses and high-end simulations.

APPROACH

Methodological developments. Develop and improve further the empirical model reduction (EMR) methodology for nonlinear stochastic inverse modeling (Kondrashov et al., 2005, 2006, 2011; Kravtsov et al., 2005, 2009), as well as other low-dimensional models (LDMs), in combination with the recently developed, past-noise forecasting (PNF) methodology for prediction (Chekroun et al., 2011). Michael Ghil, Mickaël D. Chekroun, Dmitri Kondrashov.

ENSO and coupled variability on seasonal time-scales. Improve understanding and prediction of ENSO, tropical Atlantic variability (TAV), and the Indo-Pacific coupled mode (IPT). Mark Cane, David Chapman, Chen Chen, Naomi Henderson, Alexey Kaplan, Dong Eun Lee.

MJO. Our goal in this work is to understand what kind of dynamical mode the MJO is, and what its essential ingredients are. This information will then inform prediction. Our conceptual model here is low-order models for ENSO, such as the Cane-Zebiak model, that have been so important for prediction — in their direct use as forecast models, as well as in the understanding they have generated. Adam Sobel, Daehyun Kim and Shuguang Wang.

Extratropical variability and predictability. Determine the extent to which extratropical monthly and seasonal low-frequency variability (LFV, i.e. PNA, NAO, as well as other regional blocking patterns) can be skillfully predicted for 1–12 months in advance in an LDM that includes ENSO, MJO and stratospheric linkages. Characterizate statistically extratropical storms and extremes, and link these to LFV modes. Mingfang Ting, Yochanan Kushnir, Andrew W. Robertson, Lei Wang.

Downscaling Weather and Seasonal Climate. Use LDMs to relate near-surface temperature and precipitation with predictable climate forcing such as SSTs. Explore the development of statistical tropical-cyclone (TC) forecasts based on ENSO and MJO forecasts by LDMs. Target tropical monsoon climates, emphasizing sub-seasonal characteristics of weather, such as rainfall and drought extremes. Andrew W. Robertson, Suzana J. Camargo, Yochanan Kushnir, Michael K. Tippett, John Allen.

Sea Ice. Intraseasonal and annual prediction of Arctic sea ice, improve Antarctic sea ice forecasts and assess the impact of sea ice on mid-latitude predictability. Xiaojun Yuan, Dake Chen, Lei Wang.

WORK COMPLETED

Kick-off meeting on October 6, 2012 in Palisades, NY, for UCLA and CU researchers and ONR/DoD program managers Scott Harper, Reza Malek-Madani and Fariba Fahroo.

New postdoctoral research scientists hired: John Allen, David Chapman, Chia-Ying Lee and Lei Wang (CU) and Honghu Liu (UCLA).

Workshop on Severe Convection and Climate, 3/14-15/13, Palisades, NY. Article/videos. Agenda.

Data-driven, multilayered low-order stochastic models Kondrashov et al. (2013a) introduced a general class of multilayered stochastic models (MSMs) that fall within the Mori-Zwanzig formalism of statistical physics. These models describe the role played in EMR by the non-Markovian terms that represent the cross-interactions between the resolved and unresolved variables. In EMR, such interactions appear via random difference equations forced by the resolved variables, while feeding back into the resolved dynamics via convolution integrals that involve the history of their fluctuations.

Rough parameter dependence in climate models: The role of Ruelle-Pollicott resonances Based on the spectral theory of chaotic and dissipative dynamical systems, Chekroun et al. (2013c) have shown that the recurrences observed in planetary flows can play a key role in the parameter dependence of long-term flow statistics. We interpret this dependence in terms of Ruelle-Pollicott (RP) resonances and have developed a new approach based on using Markov representations to estimate these resonances. The relation between the eigenvalues of the resulting Markov operators and the RP resonances shows that a small gap in the dominant fraction of the latter corresponds to regimes where peaks in the power spectrum are the most energetic and correlations decay slowly.

Parameterizing manifolds for stochastic partial differential equations Chekroun et al. (2013a,b) have developed a general approach for the parameterization of "small" scales in terms of the "large" ones in stochastic partial differential equations (SPDEs) by using *parametrizing manifolds* (PMs). PMs are stochastic manifolds that improve, in root-mean-square, the partial knowledge of the full SPDE solution vs. its projection onto the resolved modes. PMs are not subject to the classical spectral gap condition: they can be determined under weaker, *non-resonance conditions* on the eigenvalues associated with the resolved and unresolved modes. Non-Markovian stochastic reduced systems based on such a PM approach appear to perform outstandingly in the modeling of extreme events.

ENSO and coupled variability on seasonal time-scales. A Vector Autoregressive (VAR) model has been developed to predict tropical climate using 12 months of SST data prior to forecast initialization. The model uses SST data for the 12 months before the initialization time, and it shows particular promise for the Atlantic Hurricane Main Development Region (MDR); see Fig. 1.

Development of a low-order dynamical MJO model. We have added two new elements to the nonlinear version of the model: mixed layer ocean coupling, and weak relaxation on the moisture field. These elements represent persistent import of dry subtropical air by the Hadley circulation and the statistically stationary eddies (i.e., those not closely coupled to the MJO itself), and they allow perturbations to the model physics to change the MJO without destroying the mean state; see Fig. 2.

Analysis of MJO observations. We have analyzed MJO observations in a way designed to constrain the low-order model, in particular its moist static energy (MSE) budget. The MSE budget was analyzed using data from the equatorial Indian Ocean during the CINDY/DYNAMO field program in late 2011. This period was special because the field program obtained a number of observations not routinely available; in particular, the sounding array it deployed allows estimation of the advection terms directly from observations. We complement this with satellite-based radiation observations and large-scale estimates of surface fluxes. Some results are shown in Fig. 3.

Extratropical variability and predictability. The new post-doc, Lei Wang, joined us in September 2013. He will implement an empirical prediction model for extratropical LFV to characterize intraseasonal predictability and its seasonal dependence.

Downscaling Weather and Seasonal Climate. We have assessed the probabilistic skill of the North American Multi-model Ensemble (NMME), and have shown that regression-based correction of climate forecasts using least-squares estimates are unreliable. Our extreme index methodology — developed initially for tropical cyclogenesis and later extended to tornado activity — has been applied to hail.

Sea Ice. We have conducted empirical orthogonal function (EOF) and multivariate EOF (mEOF) analysis on the Arctic sea ice concentration and associated atmospheric variables and developed a linear Markov model to predict the principal components. We discovered and reported a teleconnection

between late-fall sea ice in the Barents-Kara-Greenland Seas and early-winter sea ice in the Bering Sea.

RESULTS

Data-driven multilayered low-order stochastic models. The structure of the MSM equations, albeit nonlinear, is such that the dynamics of the unresolved variables is orthogonal to that of the resolved ones. Likewise, the EMR formalism decomposes the dynamics of the unresolved variables across several mutually orthogonal levels. Based on these features, we developed an EMR formulation with energy-conserving nonlinearities and applied it to an idealized, partially observed, nonlinear and stochastic climate model with fully coupled slow and fast variables. The resulting energy-conserving EMR model efficiently captures the main features of the stochastic dynamics of the slow variables, even when the correlation decay times of the resolved and unresolved variables are comparable.

Reduced Markov models with state-dependent noise, and Ruelle-Pollicott resonances. This result relies on appropriately representating the dynamics by Markov operators adapted to a given observable. Such operators correspond to Markov reduced models with state-dependent noise that reflects the statistics of the unobserved variables. We have shown the model statistics of an intermediate-complexity ENSO model become more sensitive to parameter changes as the spectral gaps of the associated Markov operator become smaller: small gaps correspond to regimes where peaks in the power spectrum are the most energetic, while correlations decay more slowly.

ENSO and coupled variability on seasonal time-scales. Figure 1 (left) shows the correlation between the NOAA OISST and CFSv2 predictions of Atlantic SST in the MDR for Jan. 1982–Dec. 2010; this panel is reproduced from Fig. 9 of Hu et al. (2013). Figure 1 (right) shows the same statistic for predictions from the new VAR model (Lee et al., in prep.). The statistical model, which uses only global SST data over the year preceding the forecast initial date, outperforms CFSv2, one of the better participants in NMME. Note that VAR is generally more skillful at longer leads. In particular, for the months of strongest hurricane activity (Aug.-Sept.-Oct.), VAR out-predicts CFSv2 and has a useful level of skill for eight or more months ahead.

Development of a low-order statistical MJO model. Kondrashov et al. (2013b) performed a PNF-based predictability study of the MJO and found that PNF considerably improves predictions of the MJO phase. Even when forecasts are initiated from weak MJO conditions, useful skill is maintained out to 30 days. PNF also significantly improves the skill for initial states associated with an MJO phase over the Indian Ocean.

Development of a low-order dynamical MJO model. The recent modifications in our model resulted in a new capability to simulate the MJO in a nonlinear framework, as an organic outgrowth of a tropical climate that contains longitudinal asymmetries. With a warm pool imposed by zonally varying ocean heat transport, we can now simulate persistent eastward-propagating disturbances in the presence of a reasonable mean state (Fig. 2). A still preliminary, but crucial scientific conclusion is that ocean coupling may play a role even when the SST anomalies are very small.

Analysis of MJO observations. Observational analysis supports our LDM and provides indications for its improvement. Variations in radiative heating are in phase with precipitation and MSE, and are larger than those in surface turbulent fluxes, which lag precipitation. Radiative cooling emerges as the dominant process driving MJO instability. Vertical advection acts to damp the MJO, consistent with a positive gross moist stability, as assumed in our model. Furthermore, recent analysis supports our

hypothesis that the MJO is a "moisture mode" in the Indian Ocean, but transitions to a more Kelvin wave-like disturbance as it crosses the Maritime Continent (Sobel and Kim, 2012).

Extratropical variability and predictability. We have carried out a preliminary study to determine the preferred region of summer heat wave activities in both the current climate and the future climate. In this study, we examined the monthly mean temperature variance in seven state-of-the-art coupled ocean-atmosphere models participating in CMIP5, along with data from the NCEP/NCAR reanalysis (Fig.4). The Eurasian continent as well as North America are regions of large variability in both models and observations, although the North American patterns differ between observations and models.

Downscaling climate to weather extremes. We have continued our use of a regression-based index to downscale tornado activity from atmospheric variables and have found interannual simulation skill on regional scales (Table 1). Preliminary results applying the methodology to hail are encouraging.

Subseasonal to seasonal monsoon predictability of daily weather statistics. Moron et al. (2012) related daily rainfall characteristics during the Indian summer monsoon to an interannually modulated annual cycle (MAC) and a 30–60-day intraseasonal oscillation (ISO). We have extended this work with the purpose of assessing the impact on rainfall of predictability inherent in these modes (manuscript in preparation). We have also explored three-way interactions between the Indian monsoon, the North Atlantic, and the tropical Pacific, showing that the individual records exhibit highly significant oscillatory modes with spectral peaks at 7–8 yr, as well as in the quasi-biennial and quasi-quadrennial bands (Feliks et al., 2013).

We have further quantified the role of the MJO and ENSO in subseasonal-to-seasonal predictability, by analyzing hindcasts from three global ensemble prediction systems (EPS). The results support the concept that "windows of opportunity" for high forecast skill do exist (manuscript in preparation). A multiscale-modeling framework for daily rainfall was applied to the winter season in Northwest India. Our findings help clarify the sequence of Northern Hemisphere mid-latitude storms bringing winter rainfall over Northwest India, and their association with potentially predictable low-frequency modes on seasonal time scales and longer (Pal et al., 2013).

Sea ice. EOF and mEOF analysis of Arctic sea ice concentration (Figs. 5 and 6) reveal spatially coherent patterns in the in the Baffin Bay and in the Barents, Kara and Greenland Seas, in the Atlantic sector of the Arctic, and in the Bering and Okhotsk Seas, in the Pacific sector. The dominant signal is the long-term declining trend in the Arctic basin. We developed a linear Markov model to predict the principal component of each mEOF mode that out-performs persistence, in particular at lead times longer than 2–4 months (Fig. 7). Sea ice thickness information contributes most to the hindcast skill, followed by SST and surface air temperature (Fig. 7). Moreover, during winter and spring, most of the hindcast skill comes from marginal sea ice, particularly in the Atlantic sector of the Arctic, while the central Arctic basin is more predictable during summer and fall (Fig. 8). Sea ice concentration in the Atlantic sector is much more predictable than in the Pacific sector (Figs. 7 and 8).

A teleconnection between late fall sea ice in the Barents-Kara-Greenland Seas and early-winter sea ice in the Bering Sea is facilitated by an atmospheric Rossby wave generated by a fall sea ice anomaly in the former. It is this anomaly that creates anomalous cold advection near the Bering Sea in early winter. This teleconnection was robust in the 1980s and 1990s, but it broke down after 1998, when sea ice reduction in the Barents-Kara-Greenland Seas started to accelerate (Yang and Yuan, 2013).

IMPACT/APPLICATIONS

RELATED PROJECTS

Methodological developments. The work on the EMR and MSM methodology carried out under ONR-MURI funding is complemented by work performed with NSF-DMS–led support in the framework of an NSF-DOE-DOA program on Earth System Modeling. The latter work, under the same Lead PI, concentrates on climate sensitivity; it involves two other universities besides UCLA, namely Indiana University and the University of Nevada, Reno, as well as additional Co-PIs at UCLA. The present work concentrates on prediction and the two projects benefit strongly from each other, including the joint support of a post-doc (Honghu Liu).

MJO. The work described herein is complementary with two of our other projects. One project, funded by the NASA Modeling and Analysis Program, involves simulation of the MJO in the NASA GISS climate model. Another, funded by the NSF Large-Scale Dynamics program, involves cloud-resolving simulation of the MJO. The present project is distinct from those two in its explicit focus on development of a low-order model, as opposed to simulation with comprehensive "full-physics" models (GCM for NASA, CRM for NSF).

Extratropical variability and predictability. We also examined intensity and position changes of subtropical highs during northern summer in 20th-century observations and in 21st-century model simulations (Li et al., 2012). We found that the enhancement of subtropical highs, which can contribute to the increase in LFV of surface temperatures, is likely to be caused by enhanced land-ocean heat contrasts in the future. In another related study, we examined near-term changes in Southwestern United States hydroclimate and the mechanisms that may lead to these changes (Seager et al., 2013).

Downscaling Weather and Seasonal Climate. Our work on tornado and severe weather downscaling is also supported by a Research Initiative in Science and Engineering Award from Columbia University, on "Towards Long-Range Prediction of Tornado Activity."

REFERENCES

Chekroun, M., D. Kondrashov, and M. Ghil, 2011: Predicting stochastic systems by noise sampling, and application to the El Niño-Southern Oscillation. *Proc. Natl. Acad. Sci. USA*, **108**, 11 766–11 771, doi:10.1073/pnas.101575.

Chekroun, M. D., M. Ghil, H. Liu, and S. Wang, 2013a: On stochastic parametrizing manifolds: Stochastic bifurcations and phase transitions. *In preparation*.

Chekroun, M. D., H. Liu, and S. Wang, 2013b: On stochastic parametrizing manifolds: Pullback characterization and non-Markovian reduced equations. Submitted.

Chekroun, M. D., J. D. Neelin, D. Kondrashov, J. C. McWilliams, and M. Ghil, 2013c: Rough parameter dependence in climate models: The role of Ruelle-Pollicott resonances. *Proc. Natl. Acad. Sci. USA, sub judice*.

Feliks, Y., A. Groth, A. W. Robertson, and M. Ghil, 2013: Oscillatory Climate Modes in the Indian Monsoon, North Atlantic, and Tropical Pacific. *J. Climate*, in press.

Hu, Z.-Z., A. Kumar, B. Huang, W. Wang, J. Zhu, and C. Wen, 2013: Prediction skill of monthly SST in the North Atlantic Ocean in NCEP Climate Forecast System version 2. *Clim. Dyn.*, **40**, 2745–2759, doi:10.1007/s00382-012-1431-z.

Kondrashov, D., M. D. Chekroun, and M. Ghil, 2013a: Data-Driven Model Reduction by a Multilayered Stochastic Approach with Energy-Preserving Nonlinearities. *Physica D.*, submitted.

Kondrashov, D., M. D. Chekroun, A. W. Robertson, and M. Ghil, 2013b: Low-order stochastic model and ”past-noise forecasting” of the Madden-Julian oscillation. *Geophys. Res. Lett.*, accepted.

Kondrashov, D., S. Kravtsov, and M. Ghil, 2006: Empirical mode reduction in a model of extratropical low-frequency variability. *J. Atmos. Sci.*, **63**, 1859–1877.

Kondrashov, D., S. Kravtsov, and M. Ghil, 2011: Signatures of nonlinear dynamics in an idealized atmospheric model. *J. Atmos. Sci.*, **68**, 3–12.

Kondrashov, D., S. Kravtsov, A. W. Robertson, and M. Ghil, 2005: A hierarchy of data-based ENSO models. *J. Climate*, **18**, 4425–4444.

Kravtsov, S., D. Kondrashov, and M. Ghil, 2005: Multilevel regression modeling of nonlinear processes: Derivation and applications to climatic variability. *J. Climate*, **18**, 4404–4424.

Kravtsov, S., D. Kondrashov, and M. Ghil, 2009: Empirical model reduction and the modeling hierarchy in climate dynamics. *Stochastic Physics and Climate Modeling*, T. N. Palmer and P. Williams, Eds., Cambridge Univ. Press, 35–72.

Li, W., L. Li, M. Ting, and Y. Liu, 2012: Intensification of northern hemisphere subtropical highs in a warming climate. *Nature Geosci*, **5**, 830–834.

Moron, V., A. W. Robertson, and M. Ghil, 2012: Impact of the modulated annual cycle and intraseasonal oscillation on daily-to-interannual rainfall variability across monsoonal India. *Climate Dynamics*, **38**, 2409–2435, doi:10.1007/s00382-011-1253-4.

Pal, I., A. W. Robertson, U. Lall, and M. A. Cane, 2013: Modeling Winter Rainfall in Northwest India using a Hidden Markov Model: Understanding Occurrence of Different States and their Dynamical Connections. *Clim. Dyn.*, Submitted.

Seager, R., M. Ting, C. Li, N. Naik, B. Cook, J. Nakamura, and H. Liu, 2013: Projections of declining surface-water availability for the southwestern United States. *Nature Clim. Change*, **3**, 482–486.

Sobel, A. H. and D. Kim, 2012: The MJO-Kelvin wave transition. *Geophys. Res. Lett.*, **39**, L20 808, doi:10.1029/2012GL053380.

Yang, X. and X. Yuan, 2013: The early winter sea ice variability under the recent Arctic climate shift. Journal of Climate. *J. Climate*, Submitted.

PUBLICATIONS

Barnston, A. G. and M. K. Tippett, 2013: Predictions of Nino3.4 SST in CFSv1 and CFSv2: A Diagnostic Comparison. *Clim. Dyn.*, 1–19, doi:10.1007/s00382-013-1845-2.

Camargo, S., M. Tippett, A. Sobel, G. Vecchi, and M. Zhao, 2013: Testing the performance of tropical cyclone genesis indices in future climates using the HIRAM model. *J. Climate*, Submitted.

Cane, M. and D. Lee, 2013: What do we know about the climate of the next decade? *In Food Security and Sociopolitical Stability*, C. Barrett, Ed., Oxford U. Press, In press.

Chekroun, M. D., M. Ghil, H. Liu, and S. Wang, 2013a: On stochastic parametrizing manifolds: Stochastic bifurcations and phase transitions. *in preparation*.

Chekroun, M. D., H. Liu, and S. Wang, 2013b: On stochastic parametrizing manifolds: Pullback characterization and Non-Markovian reduced equations. *Submitted*.

Chekroun, M. D., J. D. Neelin, D. Kondrashov, J. C. McWilliams, and M. Ghil, 2013c: Rough parameter dependence in climate models: The role of Ruelle-Pollicott resonances. *Proc. Natl. Acad. Sci. USA, sub judice*.

DelSole, T., L. Jia, and M. K. Tippett, 2013a: Decadal prediction of observed and simulated sea surface temperatures. *Geophys. Res. Lett.*, **40**, 2773–2778, doi:doi:10.1002/grl.50185.

DelSole, T., M. K. Tippett, and L. Jia, 2013b: Scale-selective ridge regression for multimodel forecasting. *J. Climate*, submitted.

Feliks, Y., A. Groth, A. W. Robertson, and M. Ghil, 2013: Oscillatory Climate Modes in the Indian Monsoon, North Atlantic, and Tropical Pacific. *J. Climate*.

Jia, L., T. DelSole, and M. K. Tippett, 2013: Can optimal projection improve dynamical model forecasts? *J. Climate*, submitted.

Kelley, C., S. Mohtadi, M. A. Cane, R. Seager, and Y. Kushnir, 2013: Climate Change and Political Instability in Syria. *Proc. Natl. Acad. Sci. USA*, In review.

Kirtman, B., et al., 2013: The North American Multi-Model Ensemble for Intra-seasonal to Interannual Prediction. *Bull. Am. Meteor. Soc.*, in press.

Kondrashov, D., M. D. Chekroun, and M. Ghil, 2013a: Data-driven model reduction by a multilayered stochastic approach with energy-preserving nonlinearities. *Physica D*, submitted.

Kondrashov, D., M. D. Chekroun, A. W. Robertson, and M. Ghil, 2013b: Low-order stochastic model and "past-noise forecasting" of the Madden-Julian oscillation. *Geophys. Res. Lett.*, accepted.

Lian, T. and D. Chen, 2012: An evaluation of rotated EOF analysis and its application to tropical Pacific sea surface temperature variability. *J. Climate*, **25**, 5361–5373.

Pal, I., A. W. Robertson, U. Lall, and M. A. Cane, 2013: Modeling Winter Rainfall in Northwest India using a Hidden Markov Model: Understanding Occurrence of Different States and their Dynamical Connections. *Clim. Dyn.*, Submitted.

Sobel, A. and E. Maloney, 2013: Moisture modes and the eastward propagation of the MJO. *J. Climate*, **70**, 187–192.

Sobel, A. H. and D. Kim, 2012: The MJO-Kelvin wave transition. *Geophys. Res. Lett.*, **39**, L20 808, doi:10.1029/2012GL053380.

Tang, Y., D. Chen, D. Yang, and T. Lian, 2013: Methods of estimating uncertainty of climate prediction and climate change projection. *Climate Change - Realities, Impacts Over Ice Cap, Sea Level and Risks*, B. Singh, Ed., InTech, chap. 16, 397–420, iSBN: 978-953-51-0934-1.

Tippett, M. K. and T. DelSole, 2013: Constructed analogs and linear regression. *Mon. Wea. Rev.*, **141**, 2519–2525, doi:10.1175/MWR-D-12-00223.1.

Tippett, M. K., T. DelSole, and A. G. Barnston, 2013a: Reliability of regression-corrected climate forecasts. *J. Climate*, Submitted.

Tippett, M. K., A. H. Sobel, S. J. Camargo, and J. T. Allen, 2013b: An empirical relation between U.S. tornado activity and monthly environmental parameters. *J. Climate*, submitted.

Wu, Q., Y. Yan, and D. Chen, 2013: A linear Markov model for East Asian Monsoon seasonal forecast. *J. Climate*, **26**, 5183–5195.

Yang, X. and X. Yuan, 2013: The early winter sea ice variability under the recent Arctic climate shift. Journal of Climate. *J. Climate*, Submitted.

HONORS/AWARDS/PRIZES

- Mark Cane, Columbia University, Maurice Ewing Medal of the American Geophysical Union, 2013. Sponsors: AGU and the United States Navy.
- Mark Cane, Columbia University, Elected, National Academy of Sciences, 2013.
- Michael Ghil, UCLA, Alfred Wegener Medal and Honorary Membership of the European Geosciences Union, 2012.

LIST OF FIGURES

1 Averaged correlation in the Atlantic hurricane Main Development Region (10-20N, 20-85W), stratified by leads and target months. Black contour marks the 0.5 correlation level. 11

2 A typical nonlinear model solution. Zonal wind is plotted as a function of longitudinal distance, on the x axis, and time, on the y axis. Warm colors are positive, cool colors negative. Imposed ocean heat transport is positive in the center of the domain, negative on the edges, creating a warm pool. Eastward propagating westerly wind bursts are apparent. 12

3 Top: time series of column-integrated radiative cooling, surface turbulent fluxes, and their sum, for the DYNAMO period. TRMM satellite precipitation is shown in the grey dashed curve. Radiative cooling is from the CERES satellite, surface fluxes from the OAflux data set. Second panel: time series of column-integrated horizontal advection of moist static energy, vertical advection of moist static energy, and their sum, for the DYNAMO period. TRMM satellite precipitation is shown in the grey dashed curve. Advection terms are computed from the DYNAMO sounding array. Third panel: comparison of sum of radiative and turbulent sources with total advection. Bottom panel: comparison of column-integrated MSE tendency computed directly, vs. that from the sum of all other terms in the budget. 13

4 Summer (JJA) monthly mean temperature standard deviation based on NCEP/NCAR reanalysis (top left) and seven CMIP5 models with at least three ensemble members (indicated by the number following the name of the model in each plot) for the period 1950-2000. The data is linearly de-trended before the variance calculation. 14

5 Spatial patterns of the first three mEOF modes of (from left to right) sea ice concentration, sea ice thickness, SST, surface air temperature (a), sea ice concetration, geopotential height at 200mb, zonal and meridional winds at 200mb (b), respectively. 15

6 Spatial patterns of the first three mEOF modes of (from left to right) sea ice concentration, sea ice thickness, SST, surface air temperature (a), sea ice concetration, geopotential height at 200mb, zonal and meridional winds at 200mb (b), respectively. 16

7 Hindcast skills measured by correlations between hindcast and observation in Barents Sea (a), Sea of Okhostsk (b), Bering Sea (c) and Baffin Bay as function of leading month. Each colored curve represents a hindcast experiment using different variables together with SIC. The red curve is the persistence of SIC. 17

8 Spatial distribution of hindcast skills measured by correlations between hindcasts and observations as functions of seasons and leading months. 18

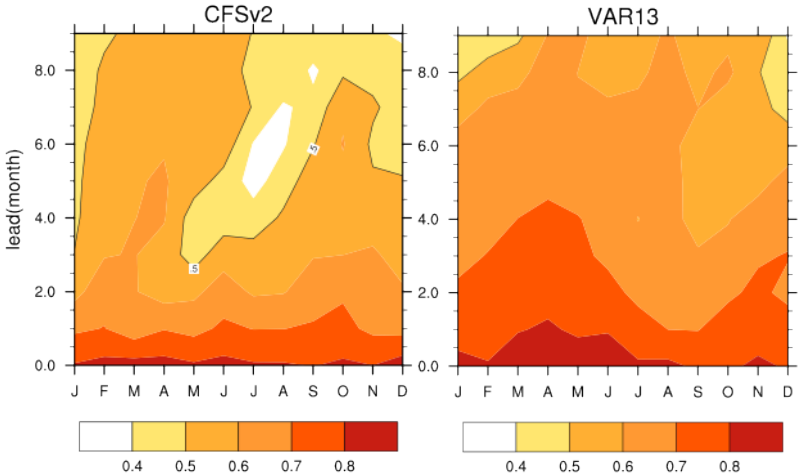

Figure 1: Averaged correlation in the Atlantic hurricane Main Development Region (10-20N, 20-85W), stratified by leads and target months. Black contour marks the 0.5 correlation level.

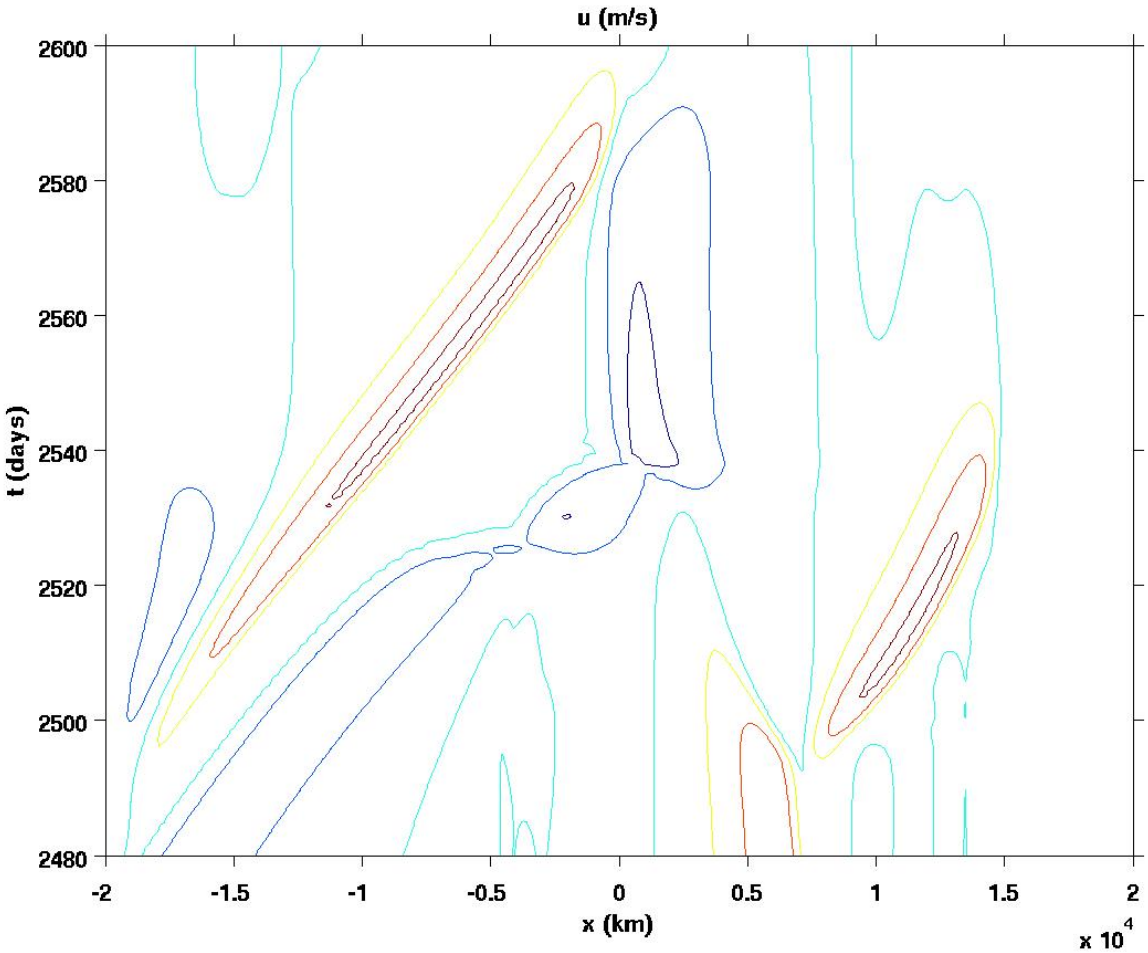

Figure 2: A typical nonlinear model solution. Zonal wind is plotted as a function of longitudinal distance, on the x axis, and time, on the y axis. Warm colors are positive, cool colors negative. Imposed ocean heat transport is positive in the center of the domain, negative on the edges, creating a warm pool. Eastward propagating westerly wind bursts are apparent.

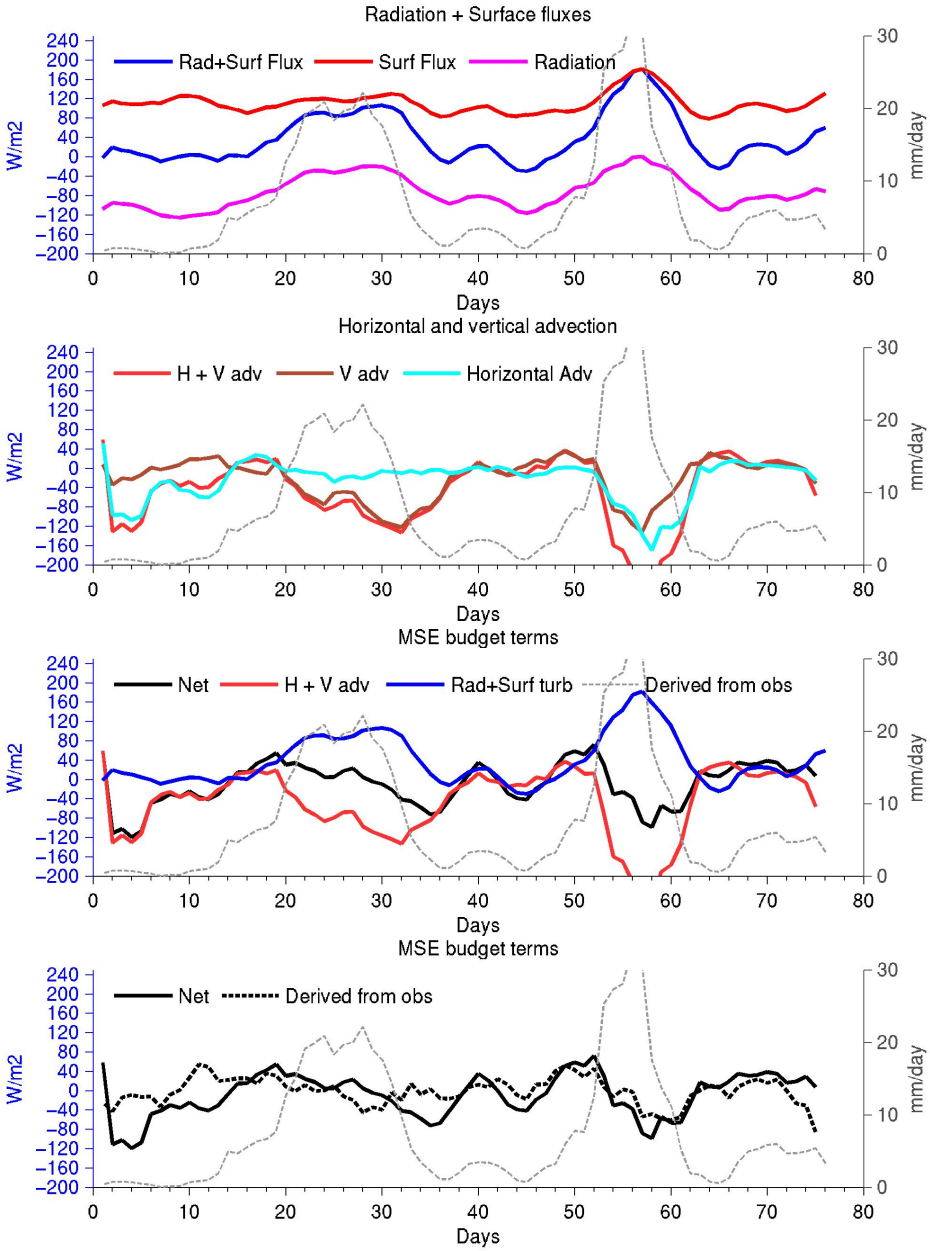

Figure 3: Top: time series of column-integrated radiative cooling, surface turbulent fluxes, and their sum, for the DYNAMO period. TRMM satellite precipitation is shown in the grey dashed curve. Radiative cooling is from the CERES satellite, surface fluxes from the OAflux data set. Second panel: time series of column-integrated horizontal advection of moist static energy, vertical advection of moist static energy, and their sum, for the DYNAMO period. TRMM satellite precipitation is shown in the grey dashed curve. Advection terms are computed from the DYNAMO sounding array. Third panel: comparison of sum of radiative and turbulent sources with total advection. Bottom panel: comparison of column-integrated MSE tendency computed directly, vs. that from the sum of all other terms in the budget.

June, July, August monthly mean temperature variability (in standard deviation) in Observations and CMIP5 Models, 1950 - 2000

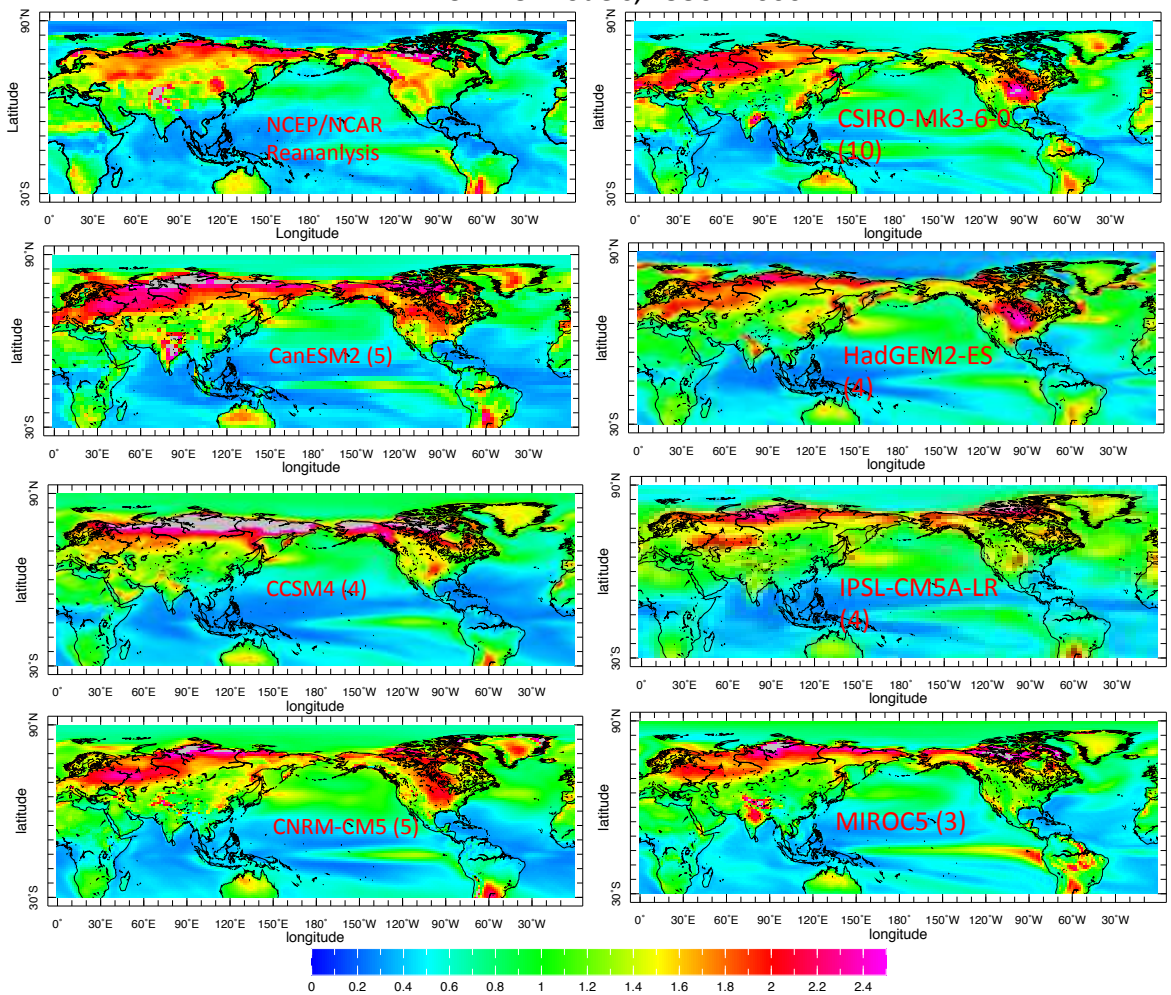

Figure 4: Summer (JJA) monthly mean temperature standard deviation based on NCEP/NCAR reanalysis (top left) and seven CMIP5 models with at least three ensemble members (indicated by the number following the name of the model in each plot) for the period 1950-2000. The data is linearly de-trended before the variance calculation.

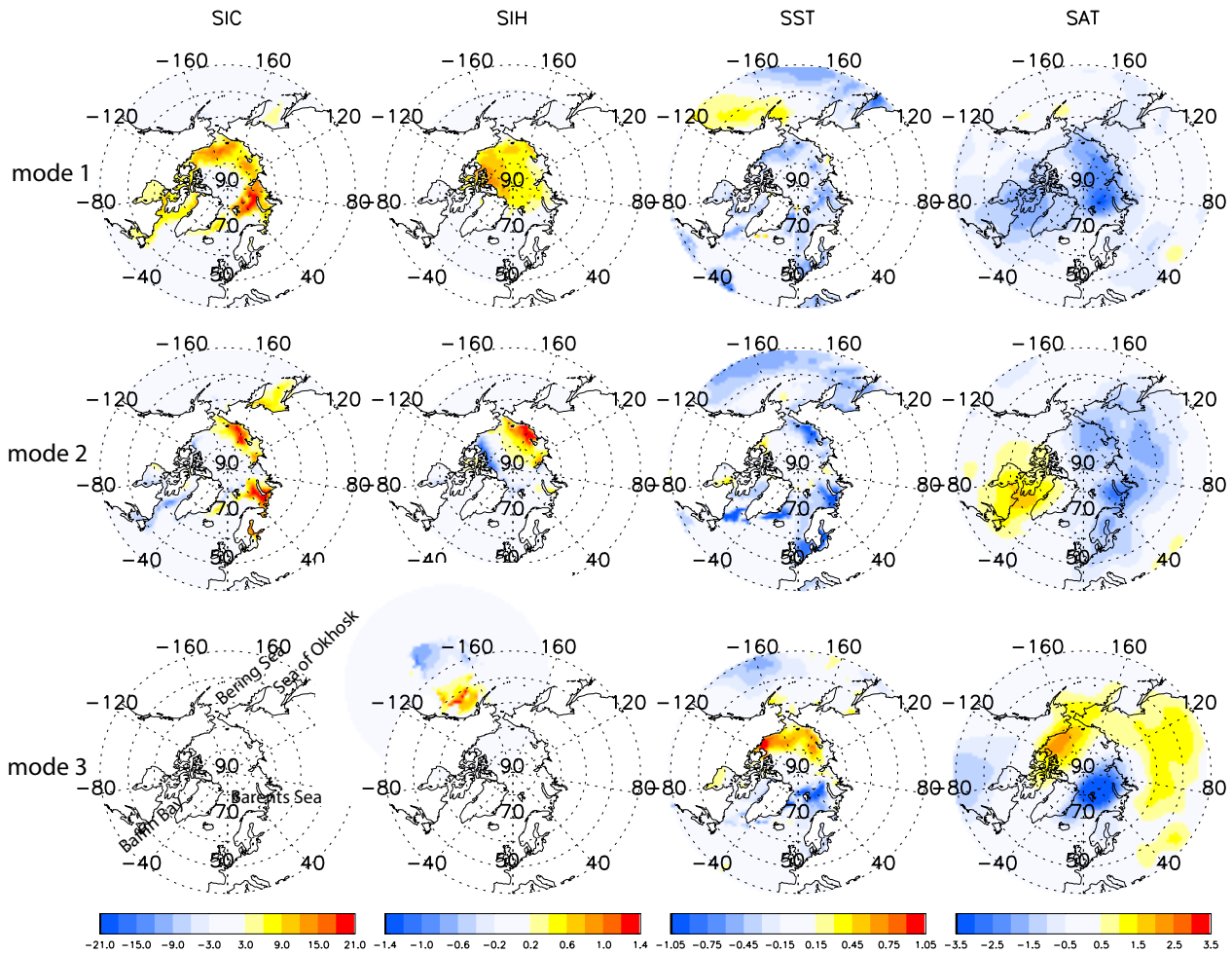

Figure 5: Spatial patterns of the first three mEOF modes of (from left to right) sea ice concentration, sea ice thickness, SST, surface air temperature (a), sea ice concetration, geopotential height at 200mb, zonal and meridional winds at 200mb (b), respectively.

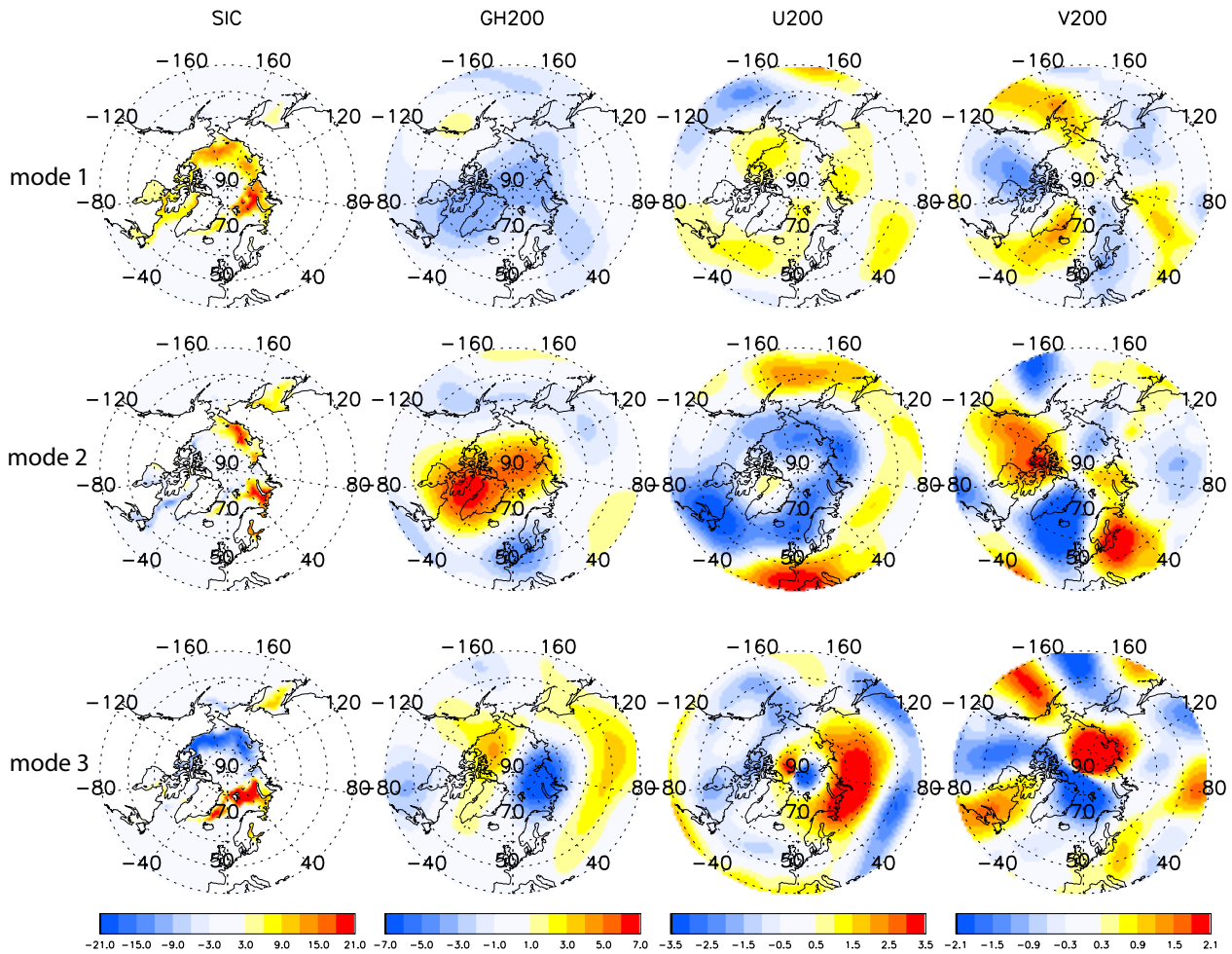

Figure 6: Spatial patterns of the first three mEOF modes of (from left to right) sea ice concentration, sea ice thickness, SST, surface air temperature (a), sea ice concetration, geopotential height at 200mb, zonal and meridional winds at 200mb (b), respectively.

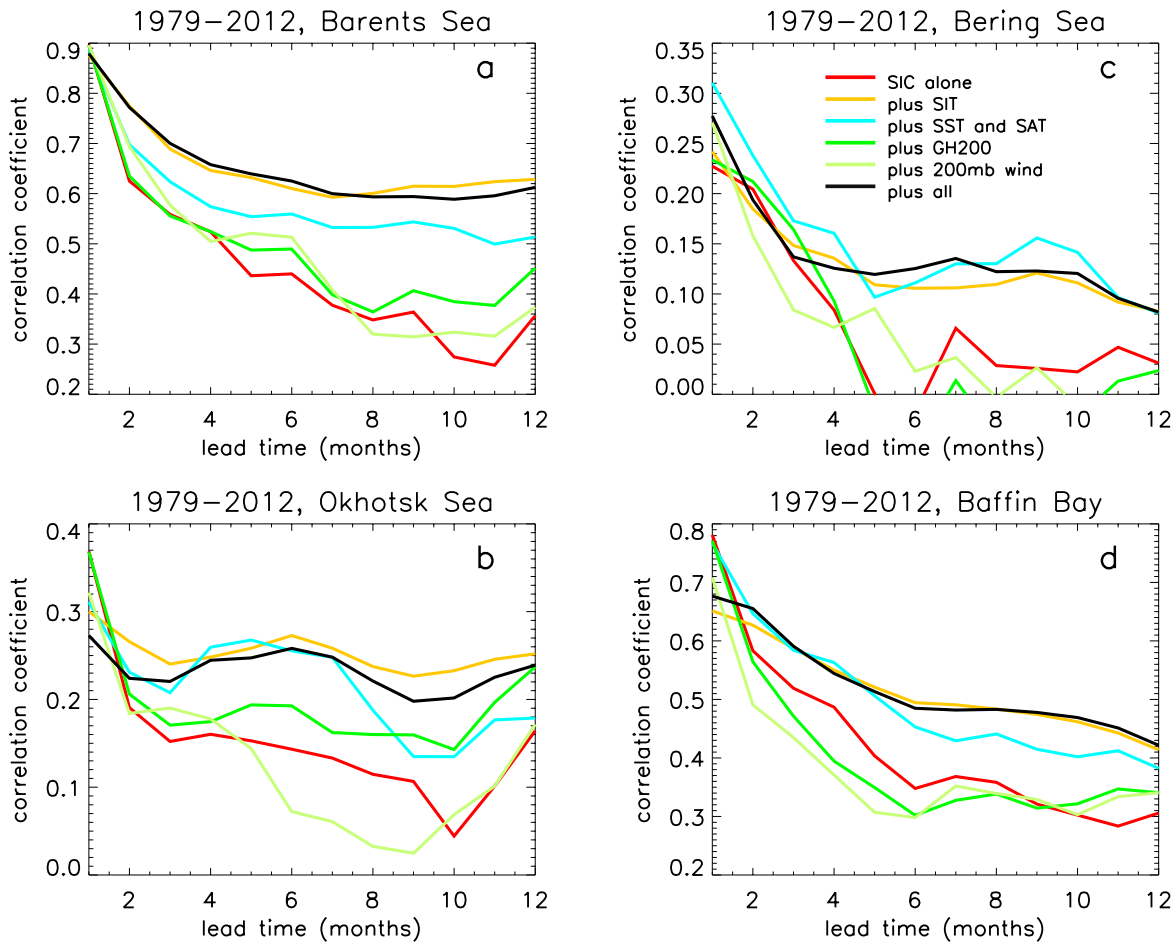

Figure 7: Hindcast skills measured by correlations between hindcast and observation in Barents Sea (a), Sea of Okhostsk (b), Bering Sea (c) and Baffin Bay as function of leading month. Each colored curve represents a hindcast experiment using different variables together with SIC. The red curve is the persistence of SIC.

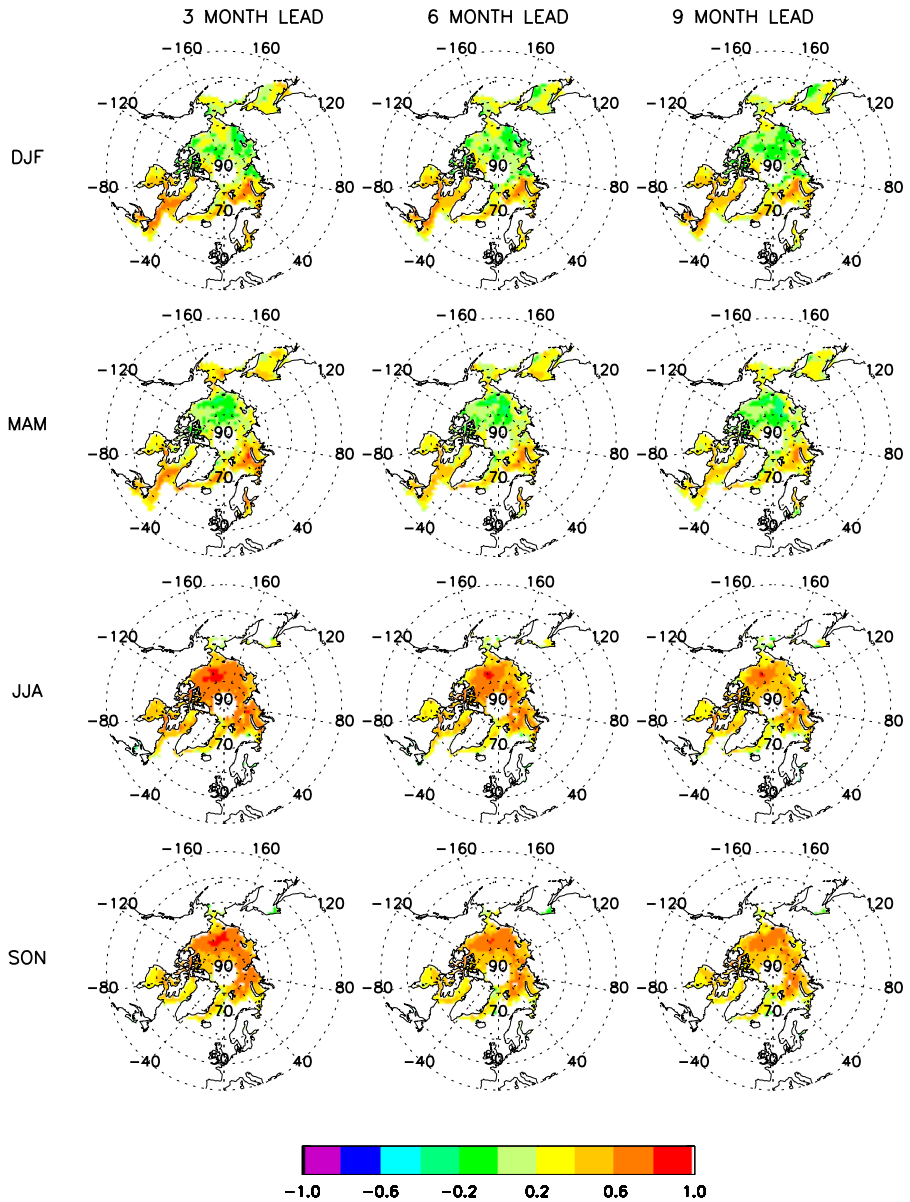

Figure 8: Spatial distribution of hindcast skills measured by correlations between hindcasts and observations as functions of seasons and leading months.

LIST OF TABLES

1 Correlation between the index and reported number of tornadoes by U.S. climate region and month for the period 1979-2010. Significant correlations are in bold font. Regions and months with less than 32 reported tornadoes during the period are omitted. 20

	Jan	Feb	Mar	Apr	May	Jun	Jul	Aug	Sep	Oct	Nov	Dec	Annual
South	**0.66**	**0.51**	**0.52**	**0.69**	**0.50**	**0.47**	**0.57**	0.31	0.12	**0.46**	**0.60**	**0.71**	**0.53**
Southeast	**0.53**	**0.54**	**0.36**	**0.47**	**0.68**	**0.46**	**0.54**	**0.42**	**0.67**	**0.41**	**0.57**	**0.69**	0.30
Central	**0.68**	**0.69**	**0.65**	**0.53**	**0.56**	**0.73**	**0.65**	0.35	**0.42**	0.26	0.28	**0.73**	**0.51**
Upper Midwest	-	-	**0.60**	**0.55**	**0.71**	**0.57**	**0.56**	0.14	**0.54**	**0.56**	-	-	**0.45**
Plains	-	-	**0.63**	**0.58**	**0.80**	**0.53**	**0.81**	**0.49**	**0.55**	0.23	-	-	**0.51**
Northeast	-	-	-	**0.38**	0.13	**0.61**	**0.50**	**0.41**	**0.37**	**0.71**	0.29	-	**0.36**
Southwest	-	-	-	0.21	0.13	**0.37**	0.32	**0.40**	0.02	0.31	-	-	0.22
Northwest	-	-	-	0.03	**0.44**	**0.36**	-	0.07	-	-	-	-	0.15
West	-	**0.49**	**0.60**	-	-	-	-	-	-	-	-	-	0.34

Table 1: Correlation between the index and reported number of tornadoes by U.S. climate region and month for the period 1979-2010. Significant correlations are in bold font. Regions and months with less than 32 reported tornadoes during the period are omitted.